Journal of Alloys and Compounds 651 (2015) 655–665

Contents lists available at ScienceDirect

Journal of Alloys and Compounds

journal homepage: http://www.elsevier.com/locate/jalcom

Transformation activity in ultrafine grained pseudoelastic NiTi wires during small amplitude loading/unloading experiments

J.L. Pelegrina [a, *], A. Yawny [a], J. Olbricht [b, 1], G. Eggeler [b]

[a] Centro Atómico Bariloche, Instituto Balseiro and CONICET, 8400 San Carlos de Bariloche, Argentina
[b] Institute for Materials, Ruhr University Bochum, 44780 Bochum, Germany

ARTICLE INFO

Article history:
Received 8 April 2015
Received in revised form
18 August 2015
Accepted 19 August 2015
Available online 21 August 2015

Keywords:
NiTi shape-memory alloys
Pseudoelasticity
Stress-induced phase transformations
R-phase
Thermal analysis

ABSTRACT

Martensitic phase transformations were studied in ultrafine grained Ni-rich pseudoelastic NiTi wires during cyclic deformation under small imposed strain amplitudes. Small strain variation tests were complemented by a thermographic analysis of the emerging temperature distributions in the specimens. The characteristics of the observed thermal profiles result from the specific phase transitions which take place at different stress levels. Homogeneous temperature changes, corresponding to a non-localized transformation activity along the specimen length, were observed throughout the whole range of applied stresses, starting from values as low as 100 MPa. This behavior is in line with previous literature reports for the stress-induced transformation from B2 austenite to R-phase as long as the critical stress for B19′ martensite formation is not reached. In the present study, similar type of transformation activity could also be demonstrated at higher strains/stresses, even after the stress induced transformation to B19′ was apparently completed. These findings suggest that transformation activity involving the B2 phase is present throughout the whole pseudoelastic stress–strain cycle; i.e., it is not restricted to the initial loading portion. Finally, non-localized transformation to or from B19′ was identified during small amplitude strain variations in the plateau-like coexistence ranges of the pseudoelastic cycle.

1. Introduction

NiTi alloys with nearly stoichiometric composition are the most used shape-memory materials due to a combination of beneficial mechanical and functional properties [1,2] which are even improved when the material is subjected to a thermomechanical treatment that induces an ultrafine grained microstructure [3]. The functional properties, such as shape memory and pseudoelasticity, have their origin in martensitic transformations between three phases. The high temperature phase, called austenite, has an ordered cubic structure of type CsCl (B2). The low temperature phase, called martensite, has a monoclinic structure (B19′). Under appropriate thermomechanical treatments, a third phase appears in an intermediate range of temperatures. It is called R-phase and exhibits a rhombohedral structure [4]. The transformations can be induced by changing the temperature (T) or by applying mechanical stresses (σ) at constant temperature. In the latter case, if T is above the minimum level for B2 being the stable phase, a stress–strain cycle as shown in Fig. 1a is observed. Starting from the B2 phase in the unloaded state (point O), the stress increases almost linearly up to about 520 MPa (point P) upon straining. It has been shown that in the stress interval O–P in Fig. 1a, the sample partially transforms from austenite to the R-phase [5,6]. From point P on, the material deforms up to about 7% strain at a constant stress level, following the path P–Q. This is due to the stress biased martensitic transformation to the B19′ phase. The mechanically induced transformation to B19′ is known to proceed heterogeneously by the movement of fronts in which the transformation is localized [7]. These interfaces sweep the sample as the imposed strain is increased until the entire specimen is transformed. The position of the fronts along the specimen can either be followed by optical observation or by detecting the thermal activity associated with the localized transformation as will be explained in more detail below. For small to moderate strain rates, one or two fronts are commonly observed to nucleate in the contact region of the specimen with the grips. They move towards the central part of the specimen with further straining. Additional nucleation events can take place along the specimen gauge length, with the number of interfaces

* Corresponding author.
E-mail address: jlp201@cab.cnea.gov.ar (J.L. Pelegrina).
[1] Now with: Federal Institute for Materials Research and Testing (BAM), 12200 Berlin, Germany.

http://dx.doi.org/10.1016/j.jallcom.2015.08.159
0925-8388/

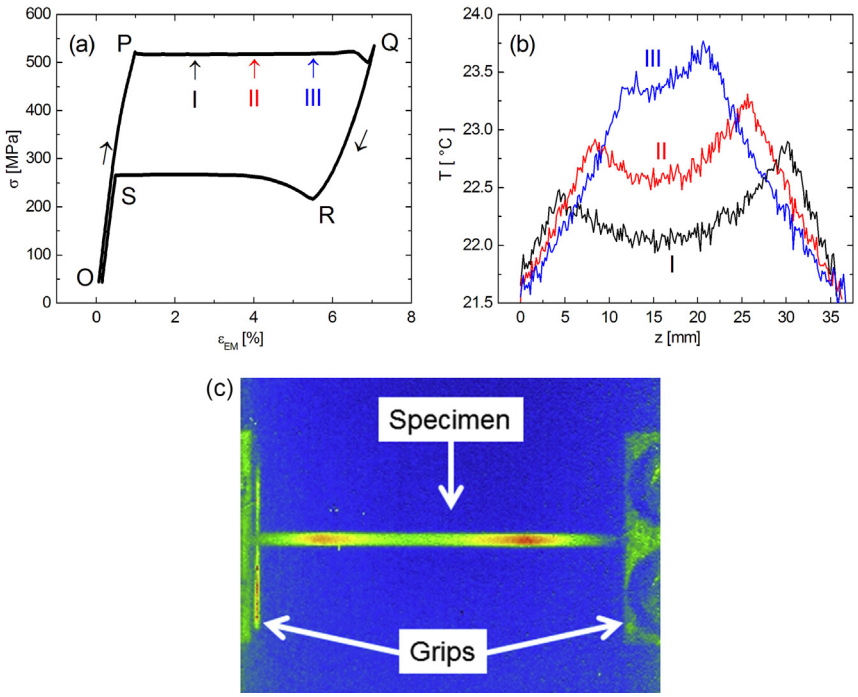

Fig. 1. Heat evolution during straining of a pseudoelastic NiTi wire specimen. (a) Stress–strain cycle with transformation plateaus (regions of constant stress) during loading and unloading. (b) Temperature profiles corresponding to the selected points I, II and III indicated in (a). (c) Representative thermograph of the wire specimen during the forward martensitic transformation corresponding to the upper stress plateau in (a).

depending on strain rate and other factors such as the dimensions of the specimen and the heat exchange with the environment [7]. If after transforming the specimen to the end of the stress plateau the strain is reverted, a roughly linear decrease of the stress from point Q to point R is first observed. The processes occurring in this portion of the cycle have not yet been clearly identified in the literature. While it was usually ascribed to elastic unloading of the phases present at point Q, it was recently postulated that this stress–strain behavior could also be associated with variant reorientation or martensite to austenite transformation [8]. Further reversion of strain results in the reverse transformation of martensite which also takes place at almost constant stress following the path R–S. A stress difference (hysteresis) between forward and reverse horizontal transformation branches of about 200 MPa is characteristic. This reverse transition proceeds too in a localized manner. As deformations of several percent can be almost fully recovered on unloading, the characteristic behavior represented in Fig. 1a is referred to as superelasticity or, alternatively, pseudoelasticity.

Since the transformations between the different involved phases are first order phase transitions, they are characterized by a latent heat which is basically determined by the enthalpy difference between the transforming phases. Thus, the temperature of the specimen changes during the transition, i.e., it increases during forward transformation (exothermic reaction) and decreases along the reverse transformation path (endothermic reaction) in the system under study. It should therefore be possible to detect any transformation activity by determining the specimen temperature profile modifications upon straining. This thermal analysis procedure can be performed with appropriate thermography camera systems [9,10]. They allow carrying out contact-free analyses of the temperature distribution at user-defined time steps during mechanical experiments. As an example, typical temperature profiles corresponding to the results shown in Fig. 1a are presented in Fig. 1b. Labels I, II, III indicate the correspondence between the profiles and the points on the pseudoelastic cycle of Fig. 1a. Two well-defined temperature peaks can be identified in the three cases. They can be associated with two transformation fronts moving towards the center of the specimen (I → II → III) as the transformation from austenite to martensite progresses along the path P–Q. These longitudinal temperature profiles of a wire specimen were obtained from thermographs like the one in Fig. 1c. Observation of profile III indicates that the two fronts collapse at a position near the center of the specimen. If the imposed strain is limited such that no severe overstressing over the upper plateau stress level occurs at point Q in Fig. 1a, it can frequently be observed that the reverse transformation takes place with two fronts first nucleating exactly at the previous collapse position [11] and then moving from the specimen center towards both ends.

The initial loading branch of the pseudoelastic cycle, path O–P in Fig. 1a, is of particular interest in the context of the present work. This zone was formerly interpreted as corresponding to the elastic deformation of the B2 phase prior to the stress-induced transformation to the B19′ phase. However, a more careful analysis showed that the stress–strain curve is not really linear and that even a small hysteresis appears on unloading from small strain values. The observed curvature was related to the transformation of austenite to R-phase [5], which is characterized by a deformation of about 1% and a mechanical hysteresis of about 10 MPa. It is worth pointing out here that results from mechanical, optical and thermal measurements reported in Refs. [6,8,12–14] show that the transformation activity in zone O–P does not proceed with distinct interfaces moving through the sample as it was the case for branches P–Q and R–S described previously.

Besides zone O–P in Fig. 1a, purely elastic deformation is also usually assumed in other zones of the pseudoelastic stress–strain cycle. For instance during loading and unloading in the zone after the transformation plateau, well on the right of Fig. 1a, or when performing small amplitude loading/unloading cycles in between the stress levels of the forward and reverse plateaus of the same

figure. The latter represents an important load situation in superelastic applications, e.g. in stents.

The aim of the present work is to establish a more fundamental understanding on the type of deformation mechanisms, i.e., elastic deformation, localized or non-localized phase transformations associated with the particular zones of the pseudoelastic cycle. With this purpose in mind, NiTi ultrafine grained wire specimens were subjected to small amplitude cycling at specific stress–strain levels and, simultaneously, thermographic analysis was performed to evaluate the transformation character. Special care was taken to avoid any movement of the localized B2/B19′ interfaces by limiting the magnitude of the imposed deformations. Based on the analysis of the mechanical and thermal response, a comparison of the transformation activity and its nature in the different zones along the wire gauge length will be presented. In addition, the measured temperature evolutions allowed estimating the different thermal transfer coefficients for the present material.

2. Experimental procedure

Ti − 50.9 at% Ni commercial wire was used (formerly Memory Metalle, Weil am Rhein, Germany). The material was hot worked, subjected to various steps of drawing and annealing, followed by a final annealing under load at about 500 °C for 60 s after a drawing reduction of nearly 50%. This treatment induces an ultrafine grained microstructure with grain size ranging from 50 nm to 150 nm which improves functional properties [6]. No precipitates were observed in transmission electron microscopy observations in the same material [6]. The wires used in the present work had a diameter of 1.2 mm and were provided with a bright surface condition after a pickling procedure.

The mechanical experiments were conducted in a MTS 858 Mini Bionix II servohydraulic machine at ambient temperature (22 °C). Wire specimens with a total length of 70 mm and a free-standing gauge length of 35 mm were used. The specimen deformation was controlled with an axial extensometer with a gauge length of 25 mm. In the present work, the strain values are indicated with subscripts CH and EM to indicate whether they were obtained from the crosshead displacement or the extensometer signal, i.e., ε_{CH} and ε_{EM}, respectively. The deformation experiments were conducted under piston displacement control using different speeds as will be described later for each specific case.

The thermographic analysis was performed in stagnant air with an infrared imaging camera VarioTHERM from Infratec Company, Dresden, Germany. This system detects wavelengths around 4 μm and the spatial and thermal resolutions are smaller than 0.2 mm (around 220 pixels along the gauge length) and 0.1 °C, respectively. The specimen surface was sprayed with a thin sub-micron graphite coating along the central 35 mm gauge length in order to enhance infrared thermal emissivity.

3. Results and discussion

3.1. Observations under non-adiabatic conditions

In the current study, the first zone considered for detailed analysis was the initial loading branch along the path O–P in Fig. 1a. The sample was subjected to a series of 20 cycles, each one consisting of four steps: a tensile displacement ramp up to a defined deformation strain (loading), a holding period at this strain, a reverse displacement ramp to a certain minimum strain (unloading), a holding period at the minimum strain. The ramps were performed at a constant displacement rate of 0.1 mm/min and the maximum elongations were progressively increased in steps of 0.01 mm in the successive cycles, starting from 0.01 mm in cycle 1 and reaching 0.20 mm in cycle 20. Holding duration was always 150 s. The last two cycles of this sequence (cycles 19 and 20) are illustrated in Fig. 2a in terms of strain ε_{CH} vs. time. The maximum

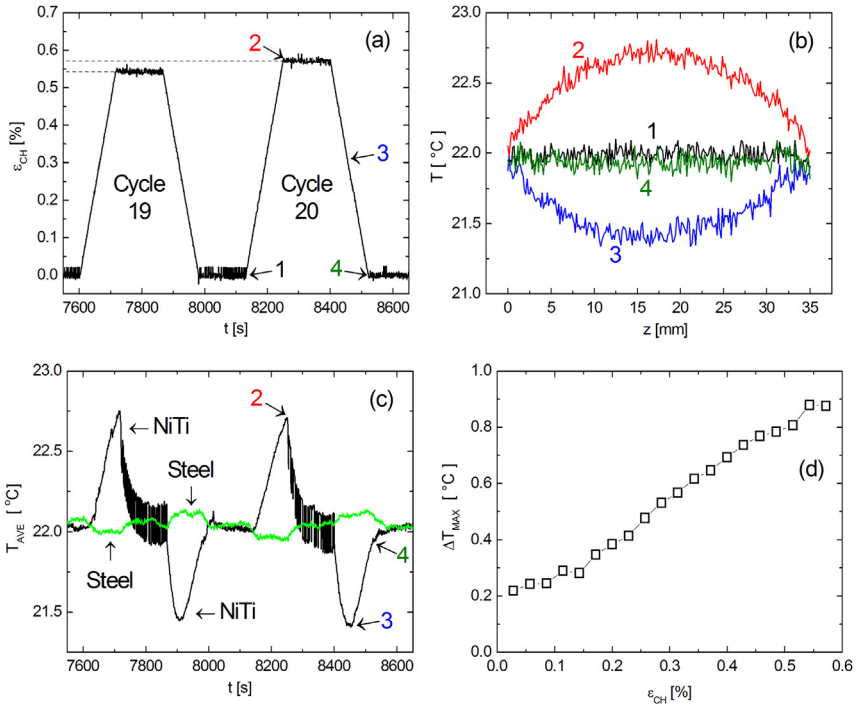

Fig. 2. Thermal effects after successive loading/unloading cycles to progressively increasing strain levels. (a) Crosshead strain resulting from imposed displacement as a function of time, (b) Temperature profiles at the selected moments indicated in (a), (c) Comparison of the mean temperature evolution in the central part of a NiTi with the thermoelastic effect in a steel specimen, (d) Maximum temperature variation (mean values from loading and unloading) in the NiTi specimen as a function of the imposed strain.

stress reached in cycle 20 was 230 MPa. This value is well below the stress level associated with the lower plateau at which the B19′ martensite would revert to austenite in the material investigated here, cf. Fig. 1a. The development of thermal activity as a consequence of the imposed strain variation is illustrated in Fig. 2b, which shows the temperature profiles along the specimen length corresponding to four specific time values of the last loading cycle (indicated by arrows and the numbers 1–4 in Fig. 2a). Temperature profile 1 corresponds to the sample in initial thermal equilibrium with ambient temperature. Profile 2 corresponds to the moment at which the displacement ramp ends and the specimen has reached the maximum strain. Clearly, the temperature increases along the whole length of the specimen as a consequence of the imposed strain. The machine's grips act as thermal reservoirs here, keeping the temperature at the specimen's ends nearly invariant throughout the experiment. This results in the temperature profiles with a parabolic shape as shown in Fig. 2b. Temperature profile 3 shows that the temperature of the specimen decreases during the unloading step. The profile 3 shown in Fig. 2b corresponds to the lowest temperature observed in this cycle. It is important to note that this was not reached at the end of the ramp but after recovering about half of the imposed deformation (in this experiment the thermographs were recorded at a frequency of 1 Hz). Profile 4 shows the situation just when the deformation is fully recovered and specimen is completely unloaded. It resembles the original isothermal condition of the specimen. The observed positive (negative) temperature variations associated with a loading (unloading) ramp can be identified with exothermic (endothermic) events or more specifically, with first order exothermic (endothermic) transformation processes. Maximum temperature variations of nearly 0.9 °C were detected (profile 2) for the central part of the specimen.

At this point, it is important to note that metals are known to exhibit the so-called thermoelastic effect, which is characterized by a temperature change occurring when the material undergoes a rapid deformation in the elastic range [15]. It must be noted, however, that the temperature variations associated with the thermoelastic effect are opposite in sign to the variations observed here, i.e., in the thermoelastic effect, cooling is observed upon loading and heating upon unloading. In the present experiments, this effect occurs simultaneously with the phase transformations involved. As it could affect the amplitude of the temperature profiles presented before by counteraction, it was decided to assess on the approximate magnitude of the thermoelastic effect for a situation similar to the given experiment. For this purpose, the same cycling sequence illustrated in Fig. 2a was applied to a steel wire in the same experimental setup. The comparison of the resulting thermal evolutions is shown in Fig. 2c. In case of the thermoelastic effect, the maximum thermal variation is opposite in sign and much smaller in magnitude when compared to the temperature variations registered for NiTi, reaching a maximum of about 0.09 °C. In spite of the differences in the material properties that determine the magnitude of the thermoelastic effect, the value obtained for the steel specimen was assumed to be a sufficient approximation for thermoelasticity in NiTi. Due to the clear difference in effects influences, the temperature variations associated with the thermoelastic effect will be neglected in the present context and the temperature variations observed in NiTi specimens will be related solely to transformation activity.

The comparison of the temperature profiles shown in Fig. 2b with those corresponding to the superelastic plateaus previously introduced in Fig. 1b indicates that a significant difference exists in the transformation characteristics. In effect, in the present case there is no indication of localized transformation activity. On the contrary, considering that the deformation rate was low and bearing in mind the “heat reservoir” effect of the grips discussed before, the profiles in Fig. 2b allow to infer that homogeneous heating occurred along the wire length. This in turn indicates that the phase transformation occurs in a non-localized way along the wire specimen.

The temperature profile sequence obtained during unloading was analyzed in terms of the lowest temperature occurring in the central part of the specimen. It turned out that the maximum temperature variation occurs at an intermediate point within the ramp (the corresponding point is labeled as 3 in Fig. 2a and c and the respective temperature profile 3 is shown in Fig. 2b). It was also proved that, at the end of the unloading ramp marked by point 4 in Fig. 2a, the sample almost reached the equilibrium temperature (point 4 in Fig. 2c and profile 4 in Fig. 2b). This fact suggests that the transformation rate (amount of transformed volume per time unit) was not constant along the imposed deformation interval. There was enough time for the specimen to reach thermal equilibrium with the environment, counteracting the effect of the endothermic transitions that were taking place during unloading. Upon loading, the temperature variation reached its maximum value at the end of the ramp as previously mentioned. It is important to consider that after each deformation step the displacement was kept constant during a holding period of 150 s to allow the sample to reach thermal equilibrium with the ambient. This can be appreciated from Fig. 2c where the average temperature (T_{AVE}) of the 3 mm central part of the specimen is plotted as a function of time for the two last cycles presented in Fig. 2a. When loading (unloading), there is an initial rise (fall) in temperature relative to room temperature. This initial temperature variation is followed by an evolution in the opposite direction, i.e. towards equilibrium with the ambient. The magnitude of the maximum temperature changes on loading and unloading coincide within the experimental scatter. Thus, the extreme temperature values (T_{AVE}) averaged over the 3 mm central portion is calculated for each cycle/strain step i ($1 \leq i \leq 20$), while the maximum variation in each cycle is obtained through the equation $(\Delta T_{MAX})_i = [(T_{AVE}^{LOAD})_i - (T_{AVE}^{UNLOAD})_i]/2$. Fig. 2d shows the values of ΔT_{MAX} as a function of the imposed strain variation in each step (ε_{CH}). It can be seen that, for low strain increments, the transformation activity is low and the related temperature increase is within the resolution limit of the thermal imaging system. For strain increments higher than 0.15%, the rise of temperature monotonously increases up to near 0.9 °C. These findings confirm recent results [6] reporting that an enhanced transformation activity occurs in the upper deformation region of the O–P zone in Fig. 1a for a similar alloy tested at ambient temperature.

The previous analysis allows drawing the following two preliminary but important conclusions. Firstly, the transformation of austenite to the R-phase occurs throughout the whole stress range corresponding to the O–P zone in Fig. 1a, including the low stress region as demonstrated by the immediate temperature rises on loading in Fig. 2c. Additionally, the stress induced transition occurs in a non-localized way along the specimen gauge length in this zone.

The parabolic shape of the temperature profiles illustrated in Fig. 2b (see profiles 2 and 3) indicates that the strain step experiments have been performed under non adiabatic conditions, i.e., heat conduction along the wire and heat transfer by convection to the ambient are modifying the otherwise flat temperature profile that would be observed under adiabatic conditions. An increase in the adiabatic character should further enhance any transformation-related thermal effects. With this objective, experiments performed at higher deformation rates are reported in the following section.

3.2. Observations under adiabatic conditions

Cycling experiments under displacement control similar to those described in the previous section (i.e., repeated sequences of loading ramp – hold time – unloading ramp – hold time) but now using a constant strain range instead of a progressively increasing maximum strain value were performed. In order to favor the adiabatic character, the displacement rate for the partial cycling was increased from 0.1 mm/min to 7 mm/min. The analysis under these new conditions was firstly repeated for the previously explored zone of nearly linear-elastic loading, path O–P in Fig. 1a, which will now be referred to as region A in Fig. 3a. In addition, the methodology was extended to regions C and M in Fig. 3a which are of particular interest. Fig. 3a includes a complete pseudoelastic cycle as a reference. It can be seen that the hysteresis loop displayed in Fig. 3a in terms of σ vs. ε_{CH} is affected by setting effects or slip of the specimen in the machine's grips, as can be identified by comparison with Fig. 1a plotted in terms of σ vs. ε_{EM}, where strain was determined by a clip-on extensometer. This is the reason for the more linear load path O–P and the lower permanent deformation at the end of the cycle observed in Fig. 1a. Cycling performed on regions A, C and M however are not affected by these types of artifacts and this can be appreciated by the corresponding cycles following stable path in Fig. 3a. The regions A and M correspond to mainly austenitic (A) and mainly martensitic (M) states, respectively, whereas coexistence of both phases is anticipated in region C. The imposed strain variation corresponded to 0.42% strain in region A and 0.44% strain in region M. The small amplitudes of deformation were chosen to ensure that no movement of interfaces was invoked in the coexistence region C. Each loading or unloading step was followed by a 150 s holding period to give the specimen sufficient time to return to room temperature T_0. Ten cycles were performed in each of the regions.

It was found that in all three cases, the strain rate was high enough to cause a homogeneous change in the temperature along the specimen. The results obtained for region A are presented in what follows in Fig. 3 while results corresponding to regions C and M will be described in detail later in Section 3.4.

Temperature profile 1 in Fig. 3b corresponds to the situation where the specimen is in thermal equilibrium with the ambient before the start of the ten displacement controlled cycles in region A. Profile 2 shows the temperature distribution just after finishing the first loading increment. The temperature profiles 3 and 4 included in Fig. 3b show the evolution towards equilibrium at a constant deformation during the subsequent holding period. A similar set of profiles is shown in Fig. 3c, now for unloading. In this case, the maximum temperature drop coincides with the end of the strain variation. The temperature profiles recorded immediately after the end of the imposed loading and unloading ramps, referred as 2 in Fig. 3b and c, respectively, exhibit nearly no curvature except for the specimen ends which are directly adjacent to the grips. This suggests predominant adiabatic conditions along almost the whole specimen gauge length. The shape of the profile coincides with the one obtained with a uniform heat source and Dirichlet type of boundary condition [16]. The maximum temperature variation that was detected approached 2 °C, which doubles the corresponding values obtained in the previous experiment. There was no evidence of temperature peaks associated to the localized motion of interfaces of the types that had been observed in Fig. 1c. The behavior just described was not affected by further cycling, i.e., similar temperature variations were measured after each of the ten applied strain cycles. The time required to reach thermal equilibrium was also found to be constant.

The results obtained in this section will be further considered in Section 3.5. Firstly, certain aspects of the thermal transfer process in the course of the evolution of the specimen temperature towards

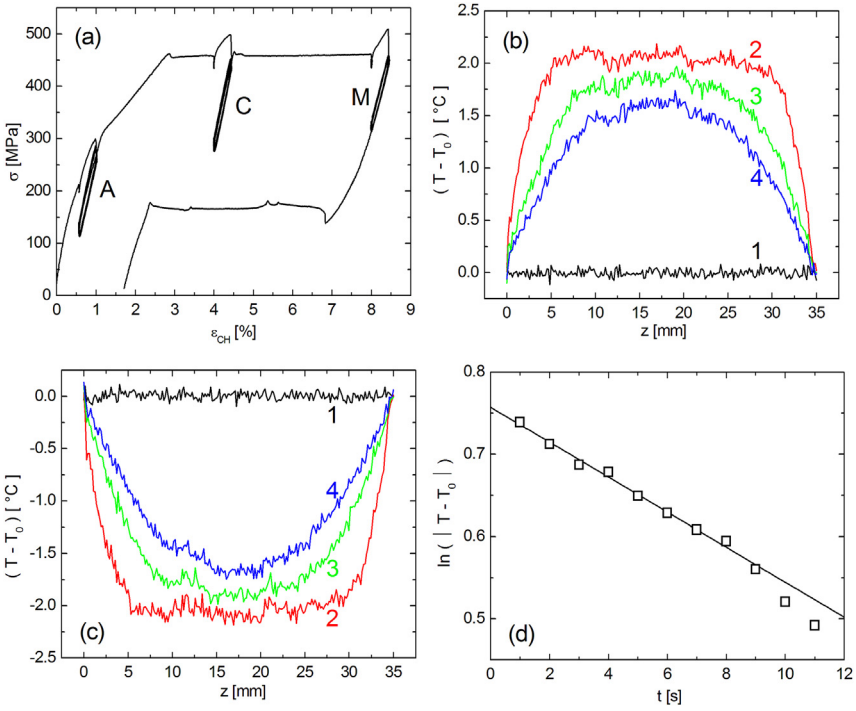

Fig. 3. Small amplitude loading under nearly adiabatic conditions. (a) Stress–strain cycle showing the regions where fast displacement controlled cycles were performed. (b) Temperature profiles obtained in region A for the thermal equilibrium condition (1, black), just after the loading (2, red), and 5 s (3, green) or 10 s (4, blue) later. (c) Similar to (b) but for the unloading branch. The graph in (d) is used to determine the decay constant for the temperature evolution due to convective heat transfer to the environment. (For interpretation of the references to color in this figure legend, the reader is referred to the web version of this article.)

equilibrium during the holding periods will be analyzed in the following section.

3.3. The evolution of the specimen temperature towards equilibrium

The present section focuses on the assessment of relevant heat transfer related coefficients, whose knowledge is necessary if a reasonable accurate modeling of the transient thermomechanical effects observed in NiTi wires is intended. Temperature profile transient effects observed during holding periods can be advantageously used for this assessment.

The temperature profiles 3 and 4 in Fig. 3b and c shows the evolution of temperature towards equilibrium at specific moments during the holding period. It can be seen that, when comparing their shapes with that of profile 2, they depart progressively from the flat shape, i.e., a curvature gradually develops in the central part. This is associated with heat transfer effects due to heat conduction along the wire and to the grips at the wire ends. Assuming a constant temperature profile along the radial direction (small Biot number, [17]), the instantaneous temperature $T(z, t)$ of a volume element located at a certain position z in this axisymmetric situation will be given by the following 1-D heat equation [17]:

$$\frac{\partial T}{\partial t} = \frac{k}{\rho\, C}\frac{\partial^2 T}{\partial z^2} - \frac{2\,h}{\rho\, C\, r}(T - T_0) \tag{1}$$

Here k represents the heat conduction coefficient, ρ the material density, C its specific heat, h is the convection heat transfer coefficient and r is the radius of the wire. This equation describes the temperature evolution to thermal equilibrium during the holding period right after the sudden variation introduced by the loading or unloading step. For this scenario, no heat sources and external work terms need to be considered.

As can be seen from Fig. 3b and c, the temperature profiles exhibit negligible second derivative in the central part of the specimen. Thus, for this central zone and for a short time interval after completing the loading ramp, the return to equilibrium is governed by heat convection to the surroundings. Thus, when applying Eq. (1) to the central position, the term carrying the second derivative can be disregarded. Solving for the temperature evolution of the central part, an exponential function with a time constant given by

$$\tau = \frac{\rho\, C\, r}{2\, h} \tag{2}$$

is obtained. Although reliable values of ρ and C can be found in the literature, values for the heat convection coefficient h are extremely sensitive to the actual conditions of the experiment. In the present setup, they might be affected by the sprayed graphite layer and this influence has to be considered when comparing experiments in the following sections. Therefore, direct determination of the value of h from the individual experimental results is the preferred option. In that way, particular values h_A for austenite can indeed be determined from Eq. (2). For this purpose, the evolution of T_{AVE} has been extracted from consecutive temperature profiles determined form the results shown in Fig. 3, both on loading and unloading. The logarithm of the absolute values of these changes as a function of time was plotted in Fig. 3d. It can be seen that the data points follow a linear relation during the first 9 s until a deviation from linearity develops for later times. The latter phenomenon can be ascribed to the increasing contribution of heat conduction which progressively reduces the extension of the linear zone in the temperature profile as it is evidenced by curves labeled by 4 in Fig. 3b and c (blue lines in the color version). The linear fit through the first nine data points presented in Fig. 3d results in $\tau = (47 \pm 2)\ s$. From this value and considering $\rho = (6450 \pm 50)\ kg\ m^{-3}$, $C = (470 \pm 20)\ J\ kg^{-1}\ K^{-1}$ [18], the coefficient h_A can be calculated from Eq. (2). A value $h_A = (19 \pm 1)\ W\ m^{-2}\ K^{-1}$ is obtained.

Appropriate values for heat conduction coefficient k are also scarce. An own evaluation is therefore intended as part of the present work. The following aspects related with the information that can be derived from the thermal analysis here performed have been taken into account. Firstly, only thermal data from the central part of the specimen was considered in order to diminish possible spurious effects associated with the influence of the grips (thermal contact resistances, mass of the grips). In addition, all analyzed data was obtained after the time period in which convection was the dominant heat transfer mechanisms i.e., only data points from time values large enough to allow a proper assessment of the second derivative of the temperature profile in the central part of the specimen were considered. The procedure consisted in evaluating the temperature profile curvature at the center at successive time increments Δt together with the corresponding temperature variations ΔT in the central part of the specimen, and then obtaining the k value through a linear fit. In this case, Eq. (1) can be expressed as:

$$\rho\, C\frac{\Delta T}{\Delta t}\bigg|_{center} + \frac{2\,h_A}{r}(T_{center} - T_0) = k\frac{\partial^2 T}{\partial z^2}\bigg|_{center} \tag{3}$$

The direct evaluation of the second derivative of the temperature profile is, however, hindered by the noise existent in the experimental data. Therefore, an alternative procedure was employed. It consisted in first approximating the temperature profile by an adequate fitting function, and then assessing its second derivative. Three alternative fitting functions were considered to test the accuracy of this approach. The corresponding equations are given by the following expressions:

$$T = A_1\left(\frac{1}{1 + e^{\frac{z-A_2}{A_3}}} - \frac{1}{1 + e^{\frac{z-A_4}{A_5}}}\right) \tag{4a}$$

$$T = A_1\left[2 - e^{-A_2(z-A_3)} - e^{-A_4(z-A_5)}\right] \tag{4b}$$

$$T = e^{A_1 + A_2\, z + A_3\, z^2} \tag{4c}$$

The coefficients A_i ($i = 1,\ldots,5$) are adjustable parameters, different for each of the proposed functions. The matching of each of the proposed fitting functions with a particular temperature profile can be appreciated in Fig. 4a. For the sake of clarity, the graphs corresponding to Eqs. (4a) and (4c) have been shifted up and down by 0.02 °C, respectively. By simple observation, it may be anticipated that the three functions fit reasonably and equally well to the experimental temperature profile. In Fig. 4b, the left term of Eq. (3), $\left(\rho\, C\,\frac{\Delta T}{\Delta t}\Big|_{center}\right)$, is plotted as a function of the second derivative of the temperature profile $\left(\frac{\partial^2 T}{\partial z^2}\Big|_{center}\right)$. A linear fit yields $k_A = (3.9 \pm 0.6)\ W\ m^{-1}\ K^{-1}$.

3.4. Observations during cycles under adiabatic conditions in regions M and D

When the wire specimen is mainly in the B19′ martensitic state before application of the “adiabatic” cycles (region M in Fig. 3a), still homogeneous temperature profiles develop (not shown here). The

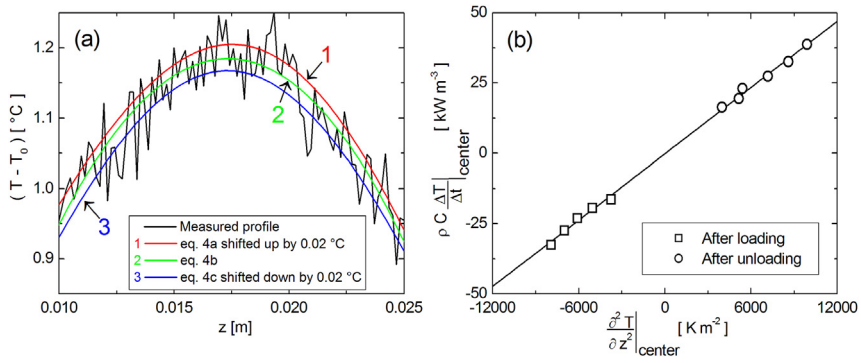

Fig. 4. Determination of the curvature of temperature profiles. (a) Correspondence of different fitting functions with the measured profile (b) Graph for the determination of the heat conduction coefficient according to Eq. (3). (Error bars in both axes are within the size of the symbols).

associated maximum temperature change however is a factor two smaller than the value obtained during cycling in region A. An evaluation similar to that performed for region A was done for region M, resulting in a heat transfer coefficient $h_M = (21 \pm 2)\ W\ m^{-2}\ K^{-1}$ and a heat conduction coefficient $k_M = (4.9 \pm 0.7)\ W\ m^{-1}\ K^{-1}$. Within experimental scatter, these values coincide with those obtained for the austenite. It is interesting to mention here that heat conduction coefficients reported in the literature for the parent phase and for martensite in NiTi are $k_A = 18\ W\ m^{-1}\ K^{-1}$ and $k_M = 8.6\ W\ m^{-1}\ K^{-1}$ [18]. However, a reduction in the heat conduction capacity similar to that obtained in the present work has been previously reported for other nanostructures in the literature [19]. There, the reduction has been related to the fact that the characteristic length scales associated to the heat carriers are comparable to the characteristic length of the nanostructures. The total thermal conductivity k can be expressed as the sum of the electronic thermal conductivity (k_e) and the phonon thermal conductivity (k_{ph}), along with any other heat-carrying mechanisms when present. It has been shown that in metals, both k_e and k_{ph} drop from their bulk values as the characteristic lengths decrease [20]. This is due to enhanced scattering of electrons or phonons as the smaller size of the sample and the grain size approach the electron or phonon mean free path, respectively.

Cycling in region C of Fig. 3 resulted in temperature evolutions that could not be determined with a precision similar to what has been done for cycling in regions A and M. This was attributed to the presence of two transformation fronts in the specimen as a result of the previous deformation. These two fronts swept the gauge length starting from both ends of the specimen, similar to the case presented in Fig. 1b. This left the austenitic part in the center of the specimen while the two martensitic zones were positioned adjacent to each of the grips, where heat conduction plays a major role. Therefore, a new specimen was tested, seeking for the presence of a single transformation front. In this case, the transition was induced from the right side until approximately one third of the gauge length was transformed to martensite. The corresponding interface position was $z = 23$ mm. In the diagrams in Fig. 5, the specimen's part on the right (between 23 mm and 37 mm) corresponds to the already stress induced B19′ martensite while the left part (between 0 mm and 23 mm) is still in a mainly austenitic (B2) condition, though in a modified one as was indicated by the measurements in the previous sections. In order to get a better impression of the heat evolution with time, the rate of data acquisition of the infrared imaging system was raised from 1 Hz to 5 Hz in this experiment. Then, cycling was started. The longitudinal temperature profiles recorded at 0.2 s time intervals during the strain reduction step are shown in Fig. 5a. It can be seen that the temperature decreased homogeneously and almost linearly in each zone of the specimen. However, the martensitic part on the right exhibits a significantly reduced variation compared to the austenitic part. The maximum temperature variations obtained on unloading for the two zones were almost 1.5 °C for the austenitic part and 1 °C for the martensitic part. While the first value is lower than the 2 °C temperature variation obtained when testing in region A, the 1 °C shift found in the martensitic zone coincides well with the value found when cycling in region M.

The equivalent results for the loading situation are presented in Fig. 5b. Again, the profiles show a homogeneous and almost linear temperature increase in the respective zones of the sample during the strain increase. The thermal activity is opposite but of similar magnitude than on unloading. It is noteworthy that the adiabatic behavior was well established and flat temperature plateaus were therefore found on each side of the retained transformation front.

In Fig. 5c and d, the evolution of the thermal profiles to equilibrium is displayed for four selected times after the maximum temperature change upon unloading/loading (profiles denoted with number 2) was reached. In this experiment, the evolutions are more complex than in specimens with a single phase state as it was the case when cycling in regions A and M. The non-homogeneous temperature distribution in the moment when loading/unloading was discontinued now causes asymmetries in the following profiles, with peak values that are positioned left of the specimen's center.

Shortly summarizing all findings reported so far, it may be concluded that clear indications are now available for non-localized phase transformation events that occur everywhere within a NiTi specimen when small strain variations are imposed to it. Interestingly, the occurrence of this non-localized transformation is completely independent of the actual material condition (austenitic, martensitic or coexistence of both phases) as characterized by the position within the pseudoelastic cycle. The intensity of the transformation activity is however clearly position dependent as could be concluded from the varying magnitude of the maximum temperature variations. Both observations give rise to the fact that heterogeneous transformations (with associated stress plateaus and moving fronts) cannot be reasonably regarded simply as step-like transitions from a 0% to 100% transformed condition. Instead, considerable transformation activity takes place in the “linear” load paths at stresses either below or above the plateau stresses. In the following section, the nature of the involved transformations and the transformed volume fraction will be further analyzed.

3.5. Determination of the transformation sequences and transforming volume fractions

The exact nature of the transformations that may be responsible for the behavior observed in Figs. 3 and 5 has not been investigated

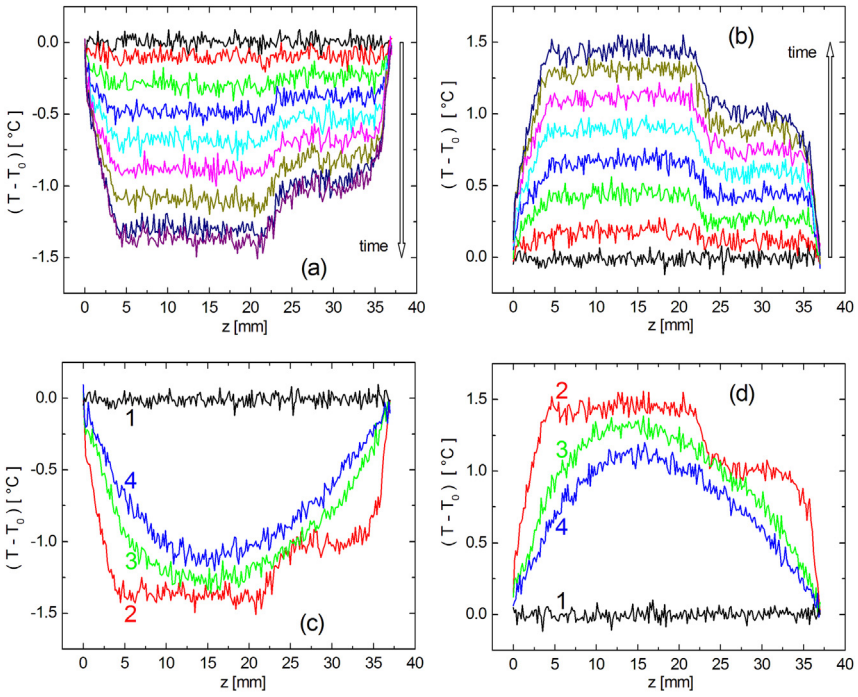

Fig. 5. Temperature profiles obtained in region C (coexistence state). (a) Sequence of profiles taken each 0.2 s showing the deviation from equilibrium on unloading. (b) Similar to (a), but on loading. (c) Profiles immediately after the end of the unloading step (2, red), and 5 s (3, green) and 10 s (4, blue) later, showing the evolution towards the thermal equilibrium profile (1, black). (d) Similar to (c) but obtained right after loading. (For interpretation of the references to color in this figure legend, the reader is referred to the web version of this article.)

so far. As the pseudoelastic NiTi wires are known to transform in a two-step transition, different individual steps need to be considered for the loading or "forward" transformation: B2 (austenite)/R-phase, R-phase/B19′ (martensite), B2 (austenite)/B19′ (martensite). In the following sections, these transformation steps will be denoted with subscripts AR, RM and AM, respectively. The analysis will be based on the adiabatic thermal response presented before.

The observed maximum temperature change ΔT_{MAX} upon an imposed strain variation can be associated with the amount of material involved in the different transformations that might be taking place. In the case of an adiabatic process, the energy balance can be expressed as

$$\sum_i m_i \, \Delta H_i = M_H \, C \, \Delta T_{MAX} \tag{5}$$

being m_i the mass undergoing a transition of type i (with i = AR, RM or AM) within a homogeneously heated zone of length L_H; ΔH_i the corresponding transformation enthalpy and $M_H(=\rho\pi r^2 L_H)$ the total mass of the zone. The length L_H of each zone will be appraised from Figs. 3 and 5, and is always smaller than the complete gauge length L of the specimen. Similarly, considering the contributions of the individual transformation strains ε_i as additive, it can be postulated that the strain variation due to all the transitions that might be present is given by:

$$\Delta\varepsilon_{Tran} = \sum_i \varepsilon_i \frac{m_i}{M_H} \tag{6}$$

The transformation strains ε_i can be obtained from the Clausius–Clapeyron type of equation of the specific transformation:

$$\frac{d\sigma}{dT} = -\frac{\Delta H}{V \, \varepsilon \, T_0} \tag{7}$$

where T_0 is the equilibrium temperature between the corresponding phases, while the slope $d\sigma/dT$ is taken from the experimentally determined linear dependence of the respective transformation stresses with temperature. A calculated specific volume $V = 8.253\ cm^3\ mole^{-1}$ was adopted as constant for all phases. The other required parameters were taken from literature and are listed in Table 1. The transformation enthalpy and strain of the transition from the R-phase to B19′ were estimated from the equations:

$$\Delta H_{RM} = \Delta H_{AM} - \Delta H_{AR}$$

$$\varepsilon_{RM} = \varepsilon_{AM} - \varepsilon_{AR} \tag{8}$$

This assumption allows working with only two unknowns in Eqs. (5) and (6), namely $m^+_{AR} = m_{AR} + m_{AM}$ and $m^+_{RM} = m_{RM} + m_{AM}$. This situation will hinder in some cases the precise determination of the kind of transformation that is operating, as will be shown next.

Table 1
Selected values for the evaluation of Eq. (7).

		Austenite/R-phase	Austenite/B19′
$\frac{d\sigma}{dT}$	$\left[\frac{MPa}{K}\right]$	18 [6]	6 [6]
−ΔH	$\left[\frac{J}{g}\right]$	6 [21]	19 [22]
T_0	[K]	300 [6]	250 [6]
ε	[−]	0.0072	0.0819

In order to allow a precise temperature measurement with the infrared camera system, all previous experiments were performed without an extensometer attached to the specimen that would have covered parts of the gauge length and would cause distortions of the thermal profiles. As a consequence, the term $\Delta\varepsilon_{Tran}$ had to be obtained from the experiments, assuming the proper deformation behavior. Fig. 6 shows the models considered which take into account different mechanisms that could be acting during the test, contributing to the measured overall strain variation $\Delta\varepsilon_{Meas}$. Their conceivable contributions to strain are given by:

- $\Delta\varepsilon_{Mach}$, the strain due to the deformation of the loading chain and grips which affects the piston displacement recorded here;
- $\Delta\varepsilon_{Elas}$, due to the elastic response of the sample, which will be taken as that corresponding to the phase with higher volume fraction;
- $\Delta\varepsilon_{AR} = \varepsilon_{AR}\frac{m^{+}_{AR}}{M_H}$ and $\Delta\varepsilon_{RM} = \varepsilon_{RM}\frac{m^{+}_{RM}}{M_H}$, the strains associated with the two transformation steps in ultrafine grained NiTi;
- $\Delta\varepsilon_{Reor}$, the additional strain contribution that might result from the reorientation of martensitic variants during the variation of the load.

Note that $\Delta\varepsilon_{Tran} = \Delta\varepsilon_{AR} + \Delta\varepsilon_{RM}$ is the magnitude to be determined in order to allow the assessment of the transforming volume fraction and kind of transition in the different loading cases. The models will now be applied to each of the regions where loading experiments were performed.

In region A of the stress strain cycle, reorientation of martensite is disregarded because the amount of variants is small and they are prone to transform back to austenite instead of reorienting. In this case, model “a” in Fig. 6 applies. From the experimental curves, a strain variation $\Delta\varepsilon_{Meas} = 0.0042$ and a stress variation of 147 MPa were determined. The elastic modulus of the austenite was obtained in a wire of similar characteristics using the lattice deformation measured with synchrotron radiation [23]. Its value of 57 GPa allows to estimate the elastic strain contribution as $\Delta\varepsilon_{Elas} = 0.0026$. The strain variation due to R-phase transformation in this region has been investigated in detail by high precision extensometer measurements, involving similar specimen material and experimental conditions as in the present tests (see Figs. 10 and 11 of [6]). The cycling stress range in region A of Fig. 3a can be associated with a transformation strain contribution $\Delta\varepsilon_{Tran} = 0.0010$, as deduced from the stress–strain room temperature curve of Fig. 11 in Ref. [6]. This assessment allows to determine the contribution of load chain deformations as $\Delta\varepsilon_{Mach} = 0.0006$, which will be used later as a rough estimate. Thus, with $L_H = 24.6\ mm$ and a maximum temperature variation of 2 °C, Eqs. (5) and (6) can be rewritten as:

$$6\ m^{+}_{AR} + 13\ m^{+}_{RM} = 0.1687\ J$$

$$0.0401\ m^{+}_{AR} + 0.4162\ m^{+}_{RM} = 0.0010 \quad (9)$$

Within experimental scatter this system has solutions $m^{+}_{AR} = 0.028\ g$ and $m^{+}_{RM} = 0\ g$.

The latter value allows deducing $m_{RM} = m_{AM} = 0\ g$ from what it turns out that $m^{+}_{AR} = m_{AR} = 0.028\ g$. This transformed mass corresponds to nearly 16% of the sample. Therefore, the heat evolution during the cycling in region A can be attributed only to the transition between austenite and the R-phase. This result is not in agreement with the observations in thin-walled tubes in Ref. [8], where the observed deformation was related to the simultaneous presence of both transitions (AR and RM). Probably, the simpler geometry of the wire, compared to the tube, allows better accommodating the R-phase-related deformation without the need of the B19′ martensite.

In region M, reorientation of the martensite acts as an additional deformation mechanism, as has been demonstrated by synchrotron diffraction in Ref. [23]. For this reason models “b” or “c” in Fig. 6 have to be used. A strain variation $\Delta\varepsilon_{Meas} = 0.0044$ and a stress variation of 128 MPa were determined from the experimental curves for region M. For the following calculation, the elastic modulus of the martensite was taken from Ref. [23]; its value of 69 GPa allows to estimate the elastic strain contribution as $\Delta\varepsilon_{Elas} = 0.0019$. If the strain contribution due to testing machine stiffness and the elasticity are subtracted from the total strain variation, a value $\Delta\varepsilon = 0.0019$ remains to be rationalized by the transformation and accommodation processes. Two deformation models (“b” and “c” in Fig. 6) are considered here which incorporate the reorientation strain contribution in different ways. Model “b” assumes a simple linear addition of all anticipated contributions, yielding the opportunity that individual contributions might play no role (i.e., reach a value of zero) while the other elements become more important. When assessing the applicability of model “b”, it is important to consider an additional condition derived from the results in Ref. [8], where it was demonstrated that the reorientation and elastic strain rates for loading of the martensitic microstructure are of the same order. Considering a reorientation contribution of similar value to the elastic strain, the application of model “b” would yield a value of $\Delta\varepsilon_{Tran} = 0$, i.e., no transformation would occur. This scenario cannot be true, since the results of the thermography clearly indicate the presence of transformation activity. Reorientation processes can be interpreted in two different ways. In one case, the initial martensite variant transforms back to austenite from which the new variant grows. This sequence implies consecutive endo- and exothermic processes which would nearly compensate, yielding a negligible heat signal. In the other case, the reorientation takes place through the movement of interfaces which separate both martensite variants. In this situation the heat signal is also expected to be low and, additionally, it should have the same exothermic (frictional) character, independently of the sense of the strain variation.

The alternative model “c” in Fig. 6 considers the reorientation process as an inherent characteristic of the martensitic transformation that is always active whenever stress variations are high enough to stimulate any transformation activity. In a first order approximation (and only for the low deformations applied here), it will be anticipated that both contributions are of similar magnitude, i.e., $\Delta\varepsilon_{Tran} = \Delta\varepsilon_{Reor} = 0.0019$, implying at the same time that

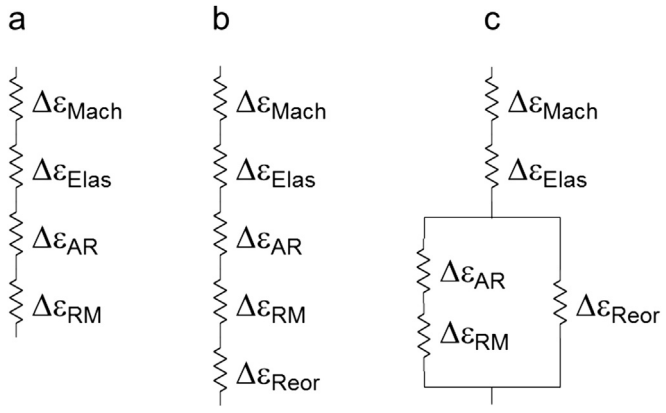

Fig. 6. Scheme of different models used to rationalize the measured strain variation during cycling. (a) Simplified deformation model for initial loading with low phase fractions of martensitic phases in the specimen, (b) and (c) models that consider additional strain contributions from self-accommodation processes in predominantly martensitic specimens. See text for further details.

also $\Delta\varepsilon_{Elas} = \Delta\varepsilon_{Reor}$ in full accordance with [8]. Then, with $L_H = 24.6\ mm$ and a maximum temperature variation of 1 °C, it holds that

$$6\ m^{+}_{AR} + 13\ m^{+}_{RM} = 0.0843\ J$$

$$0.0401\ m^{+}_{AR} + 0.4162\ m^{+}_{RM} = 0.0019 \quad (10)$$

Within experimental scatter this system has solutions $m^{+}_{AR} = 0.005\ g$ and $m^{+}_{RM} = 0.004\ g$. This means that, in region M, the heat evolution could arise from a set of different alternatives, ranging from a negligible (m_{AM} ~ 0) to a single type of transformation (m_{AM} ~ 0.005 g, nearly 3% of the sample) from austenite to B19′ martensite. In the former case, it can happen that nearly 3% of the sample transforms from austenite to R-phase and, at the same time, another 3% transforms from R-phase to martensite. The information obtained in the present experiments does unfortunately not allow a more thorough understanding of the real situation in region M.

In region C, with its peculiarity of co-existing austenitic and martensitic specimen parts, different models need to be considered for these two elements. In the following, model "a" was applied to the material being initially in austenite while "c" was used for the martensitic part. The experimental results for region C yield a strain variation $\Delta\varepsilon_{Meas} = 0.0043$ and a stress variation of 147 MPa during cycling. The austenite showed a temperature variation of 1.5 °C in a length $(L_H)_A = 17.6\ mm$, while the martensite temperature varied by 1 °C within $(L_H)_M = 9.8\ mm$. Taking the moduli of elasticity like in the above cases, this results in $\Delta\varepsilon_{Elas} = 0.0026$ for the austenitic and $\Delta\varepsilon_{Elas} = 0.0021$ for the martensitic part. The corresponding linear systems have the following solutions: $m^{+}_{AR} = 0.015\ g$ and $m^{+}_{RM} = 0\ g$ in the austenite (transforming to the R-phase nearly 12% of the corresponding volume), and $m^{+}_{AR} = 0.002\ g$ and $m^{+}_{RM} = 0.002\ g$ in the martensite. These results suggest that the transformation activity in region C, i.e. during load variation in the two-phase region within the pseudoelastic stress–strain hysteresis loop, is similar to that found for the respective regions at both extremes, but of smaller magnitude in the austenitic part. This decrease is in agreement with the change in R-phase transformation intensity with the stress level, as can be seen from the results presented in Fig. 13c of [6]. There, it was shown that the heat evolution becomes reduced at the stress range used in region C as compared to the range used in region A.

In addition to the individual transformation analyses in each of the small cycling regions, an attempt was made to reach further understanding of the processes in the initial (linear-elastic) load path by combining the different results. Note that the stress variations during cycling in regions A and D barely overlap. When they are summed up, a total stress variation is obtained representing about 80% of the (yield) stress at point P in Fig. 1a. A careful analysis of the temperature evolution in the experiments performed under nearly adiabatic conditions indicates that there is a negligible transformation activity in the lower 20% of the O–P stress interval defined in Fig. 1. Similarly, the sum of the mass fractions that transformed in region A and in the austenitic region of C can be calculated. The evaluation indicates that 27% of the sample will have transformed from austenite to the R-phase prior to the beginning of the localized transformation.

4. Conclusions

The thermal response of a commercial pseudoelastic ultrafine grained NiTi wire to cyclic mechanical loading with small strain variations was examined. The heating/cooling effects of the occurring phase transformations were analyzed by an infrared imaging system. The following conclusions can be drawn from the present study:

1 There is evidence of non-localized phase transitions already for very low values of applied stress in the 100 MPa range, i.e., in a zone that is usually assumed to represent the elastic response of the austenitic phase.
2 Little strain variations, small enough to avoid the movement of transformation fronts associated with Lüders type of localized transformation, result in transitions that occur in a non-localized way within the whole specimen. This finding is valid in unloaded, partially transformed and fully transformed conditions.
3 By performing fast loading/unloading experiments under nearly adiabatic conditions, it was possible to determine the kind of transition and transforming volume fractions during small strain variations. This quantification is particularly relevant and useful for the understanding and modeling of superelastic behavior. The transformation sequence under such loadings was by far not clear, as contributions from concurrent processes seemed possible.
4 When specimens are pre-loaded (to reach a predominantly martensitic condition) and then small strain cycles are imposed, the resulting deformation behavior and temperature variations can be rationalized by different transformation scenarios. These range from appearance of two subsequent transition steps (austenite to R-phase followed by R-phase to martensite) to the direct austenite to B19′ martensite transformation. On the contrary, this lack of certainty disappears when austenitic specimens are cyclically loaded with small applied strain variation, because only the transition from austenite to R-phase is induced.
5 Within experimental scatter, similar heat transfer coefficients of (19.4 ± 0.9) W m^{-2} K^{-1} and heat conduction coefficients of (4.3 ± 0.5) W m^{-1} K^{-1} can be deduced for both, austenite and B19′ martensite in this ultrafine grained material.
6 In ultrafine grained NiTi, more than 25% of the austenite phase may transform to R-phase prior to the onset of the heterogeneous localized transition which results in a continuous deformation at constant stress (transformation plateau). This finding underlines the importance of this often overlooked first transformation step.

Acknowledgments

The authors acknowledge funding by the Deutsche Forschungsgemeinschaft DFG, Land Nordrhein-Westfalen, and Ruhr University Bochum through the Collaborative Research Centre on Shape Memory Technology (SFB 459: Formgedächtnistechnik). AY and JLP acknowledge support from CNEA, CONICET, UNCUYO and ANPCYT (Argentina).

References

[1] J. Van Humbeeck, Non-medical applications of shape memory alloys, Mater. Sci. Eng. A 273–275 (1999) 134–148.
[2] T. Duerig, A. Pelton, D. Stöckel, An overview of nitinol medical applications, Mater. Sci. Eng. A 273–275 (1999) 149–160.
[3] A. Yawny, M. Sade, G. Eggeler, Pseudoelastic cycling of ultra-fine-grained NiTi shape-memory wires, Z. für Met. 96 (2005) 608–618.
[4] T. Saburi, Ti-Ni shape memory alloys, in: K. Otsuka, C.M. Wayman (Eds.), Shape Memory Materials, Cambridge University Press, 1998, p. 49.
[5] S. Miyazaki, K. Otsuka, Deformation and transition behavior associated with the R-phase in Ti-Ni alloys, Metall. Trans. A 17 (1986) 53–63.
[6] J. Olbricht, A. Yawny, J.L. Pelegrina, A. Dlouhy, G. Eggeler, The effect of R-phase on physical and mechanical properties of ultra fine grained Ni-rich NiTi shape memory alloys, Metall. Mater. Trans. A 42 (2011) 2556–2574.
[7] J.A. Shaw, S. Kyriakides, On the nucleation and propagation of phase

transformation fronts in a NiTi alloy, Acta Mater. 45 (1997) 683–700.
[8] D. Favier, H. Louche, P. Schlosser, L. Orgéas, P. Vacher, L. Debove, Homogeneous and heterogeneous deformation mechanisms in an austenitic polycrystalline Ti-50.8 at.% Ni thin tube under tension. Investigation via temperature and strain field measurements, Acta Mater. 55 (2007) 5310–5322.
[9] B. Krevet, V. Pinneker, M. Rhode, C. Bechthold, E. Quandt, M. Kohl, Evolution of temperature profiles during stress-induced transformation in NiTi thin films, Mater. Sci. Forum 738–739 (2013) 287–291.
[10] B. Reedlunn, S. Daly, J. Shaw, Superelastic shape memory alloy cables: part I – isothermal tension experiments, Int. J. Solids Struct. 50 (2013) 3009–3026.
[11] A. Schäfer, J. Olbricht, M.F.-X. Wagner, Monitoring localized deformation of pseudoelastic NiTi subjected to uniaxial loading, in: G.B. Olson, D.S. Lieberman, A. Saxena (Eds.), Proceedings of the International Conference on Martensitic Transformations (ICOMAT08), The Minerals, Metals and Materials Society, Warrendale, Pennsylvania (USA), 2009, pp. 537–542.
[12] L.C. Brinson, I. Schmidt, R. Lammering, Stress-induced transformation behavior of a polycrystalline NiTi shape memory alloy: micro and macromechanical investigations via in situ optical microscopy, J. Mech. Phys. Solids 52 (2004) 1549–1571.
[13] P. Feng, Q.P. Sun, Experimental investigation on macroscopic domain formation and evolution in polycrystalline NiTi microtubing under mechanical force, J. Mech. Phys. Solids 54 (2006) 1568–1603.
[14] X. Zhang, P. Feng, Y. He, T. Yu, Q. Sun, Experimental study on rate dependence of macroscopic domain and stress hysteresis in NiTi shape memory alloy strips, Int. J. Mech. Sci. 52 (2010) 1660–1670.
[15] W. Thomson, On the dynamical theory of heat, Trans. R. Soc. Edinb. 20 (1853) 261–288.
[16] S.Y. Yang, G.S. Dui, Temperature analysis of one-dimensional NiTi shape memory alloys under different loading rates and boundary conditions, Int. J. Solids Struct. 50 (2013) 3254–3265.
[17] F.P. Incropera, D.P. DeWitt, Fundamentals of Heat and Mass Transfer, fifth ed., John Wiley and Sons, Inc, 2002.
[18] J. Van Humbeeck, R. Stalmans, Characteristics of shape memory alloys, in: K. Otsuka, C.M. Wayman (Eds.), Shape Memory Materials, Cambridge University Press, 1998, p. 174.
[19] G. Chen, Particularities of heat conduction in nanostructures, J. Nanoparticle Res. 2 (2000) 199–204.
[20] N. Stojanovic, D.H.S. Maithripala, J.M. Berg, M. Holtz, Thermal conductivity in metallic nanostructures at high temperature: electrons, phonons, and the Wiedemann-Franz law, Phys. Rev. B 82 (2010) 075418 (1-9).
[21] Y. Liu, P.G. McCormick, Influence of heat treatment on the internal resistance to the martensitic transformation in Ni-Ti, in: C.M. Wayman, J. Perkins (Eds.), Proceedings of the International Conference on Martensitic Transformations (ICOMAT 92), Monterey Institute of Advanced Studies, Carmel, USA, 1993, p. 923.
[22] P.A. Besselink, Memory metal: properties and applications, in: V. Torra (Ed.), The Science and Technology of Shape Memory Alloys, Impresrapit, Barcelona, Spain, 1989, p. 407.
[23] M.L. Young, M.F.-X. Wagner, J. Frenzel, W.W. Schmahl, G. Eggeler, Phase volume fractions and strain measurements in an ultrafine-grained NiTi shape-memory alloy during tensile loading, Acta Mater. 58 (2010) 2344–2354.